LA-UR-87-1714

LA-UR--87-1714

DE87 010126

Los Alamos National Laboratory is operated by the University of California for the United States Department of Energy under contract W-7405-ENG-36.

TITLE: OPTICAL ANALYSIS OF HIGH POWER FREE ELECTRON LASER RESONATORS

AUTHOR(S): Charles, E. Knapp, CLS-8

V. K. Viswanathan, CLS-8

Quentin D. Appert, CLS-8

Steven C. Bender, CLS-8

Brian D. McVey, X-1

SUBMITTED TO: AIAA 19th Fluid Dynamics and Plasma Dynamics and Lasers Conference

Honolulu, Hawaii
June 7-10, 1987

DISCLAIMER

Los Alamos National Laboratory
Los Alamos, New Mexico 87545

OPTICAL ANALYSIS OF HIGH POWER FREE ELECTRON LASER RESONATORS

C. E. Knapp, V. K. Viswanathan, Q. D. Appert,
S. C. Bender, and B. D. McVey

University of California, Los Alamos National Laboratory
P.O. Box 1663, MS E523, Los Alamos, NM 87545
(505) 667-6065

Abstract

The first part of this paper briefly describes the optics code used at Los Alamos National Laboratory to do optical analyses of various components of a free electron laser. The body of the paper then discusses the recent results in modeling low frequency gratings and ripple on the surfaces of liquid-cooled mirrors. The ripple is caused by structural/thermal effects in the mirror surface due to heating by optical absorption in high power resonators. Of interest is how much ripple can be permitted before diffractive losses or optical mode distortions become unacceptable. Preliminary work is presented involving classical diffraction problems to support the ripple study. The limitations of the techniques are discussed and the results are compared to experimental results where available.

Introduction

This paper is a continuation of a previous one,[1] which discussed the optical analysis of a grazing incidence, optical resonator intended for use in a Free Electron Laser (FEL) at Los Alamos. The emphasis was on the comparison of the code to experiment. The present paper will continue this effort and analyze the modeling of the surfaces of liquid-cooled mirrors when high power laser beams are incident on them. The ultimate aim in these analyses is to be able to design optics needed for the FEL, which take into account the various tolerances necessary for the components of an efficient and practical system.

Presented first will be a brief discussion of the optics code, General Laser Analysis and Design Code (GLAD), used in the analysis. Next, preliminary cases are presented, consisting of classical diffraction problems, in which the code is compared to analytically derived cases. The study consisted of running the following established textbook cases: the square and circular apertures, Young's slits (two-slit problem), and the four and six slit gratings. Generally, there is very good agreement with the analytically derived values. For the four-slit case, there are some differences in the results and the disagreements increase with the increase in the number of slits analyzed. The code is limited by the finite array in the Fast Fourier Transform technique used in the code.

Following this is a report of the results of modeling ripple on liquid-cooled mirrors caused by thermal distortion. The mirror model used here assumes that the cooled mirrors have a substructure consisting of a grid of square cells through which the fluid flows. When a high power beam is incident on such a surface, the surface deformations resulting from heat absorption approximate a sinusoidal ripple across the mirror in two directions. This effect can be modeled as a very low frequency grating. The resonator configuration used for this case consisted of two normal incidence, spherical mirrors, with a grazing incidence, hyperboloidal, beam expanding mirror in between. This cavity has been described in detail and analyzed in Reference 1. The large angle of incidence (86°) at the grazing incidence mirror complicates the ripple patterns. This case has been successfully modeled.

In conclusion, it is shown that the code is successful in analyzing the low frequency ripple situations encountered in the resonator optics for the FEL. The analysis to date has already produced results which provide direction for practical design of FELs. Losses due to diffraction from the ripple could be significant.

Description of the GLAD Code and Its Application to the Optical Analysis of Free Electron Lasers

The GLAD code used in the modeling of effects described in this paper is the latest in the series of LOTS diffraction propagation codes, developed over the years. This series of codes has been developed by Applied Optics Research, the Air Force Weapons Laboratory, and the Los Alamos National Laboratory. The code uses Fast Fourier Transform and ray tracing techniques to analyze optical systems from end to end.

Historically, the codes that have been developed and used for the design and analysis of laser optical systems with resonators and tilted components have been paraxial in nature. Calculations and corrections of optical aberrations in the system were done with off-line codes and folded systems were modeled by "unfolding" the system. Such codes and techniques are inadequate to design and analyze grazing incidence resonators (with tilted components) which are encountered in the FELs of interest. These difficulties and the development of a diffraction routine with exact, ray aberration calculations for grazing incidence optics used in arbitrarily tilted and decentered systems have been described in detail in a previous paper.[2] This approach has been successfully implemented in the GLAD code and the analysis herein uses this approach.

Briefly, to describe the propagation of a beam through a complex three-dimensional optical system, the code defines four coordinate systems:

GLOBAL - Ray and vertex locations.
RAY - Complex amplitude distributions.
VERTEX - Component rotations and shape definitions.
SURFACE - Surface at chief ray intercept point.

The global coordinate system allows components to be positioned and rotated arbitrarily. Exact aberrations are calculated for components in aligned or misaligned configurations by using ray tracing to compute optical path differences and diffraction propagation. The optical path differences between components and beam rotations in complex mirror systems are calculated accurately.

The code has a modular structure and is therefore very versatile in nature. User defined modules are also permissible, such as a single pass through a fully three-dimensional resonator cavity. These modules can then be called any number of times. Thus, the GLAD code enables the determination of the properties of the optical beam passing many times through a very complicated FEL system. The next sections describe the results obtained using this code for the problems studied.

Comparison of Code to Classical Problems

Preliminary cases were run to demonstrate that the code is working correctly. These cases consist of modeling square and circular apertures and comparing the results to the expected sinc^2 function ($\text{sinc}(x) = \sin(x)/x$) and to the Airy pattern, respectively. These examples are found in Born & Wolf[3] and Schaums Outline Series on Optics.[4]

The square aperture case, as set up to run on GLAD, consisted of a plane wavefront impinging normally on a square aperture (0.4 cm x 0.4 cm), which was then propagated through a lens of focal length 5000 cm and then to the focal point. To obtain the best agreement required the use of a large array (256 x 256). For the circular case the setup was the same except for the aperture, which was 0.4 cm in diameter. The wavelength used was 0.65 μm.

The comparison of the GLAD results to the sinc^2 function showed very good agreement. The amplitude of the first diffraction lobe agreed to within 1.2% of the theory. The second lobe had a 1.0% error and the third lobe had an 8.0% error. For the circular aperture, agreement of the code with the Airy pattern was very good for the first diffraction ring, (0.4% error). The agreement for the second and third rings was not as good with errors of 10.% and 14.% respectively.

The next set of cases was multiple slit problems (two, four, and six slits), again chosen from text book examples[4] in an attempt to tie the code results to those of well known problems which have been verified by experiment.

The two-slit case, also known as Young's experiment, as set up for the code, has slit widths of b = .01 cm and a slit separation of a = .05 cm. The slit separation is measured between the middles of the two slits. The expected result is a series of fringes under an envelope of the sinc^2 function. The quantity M = a/b predicts which fringes will coincide with the minima of the sinc^2 function and hence will be missing. For this case, every fifthth fringe should be missing. After judicious selection of the unit size for the array spacing between points, very good agreement was obtained with theory; the fifth, tenth, fifteenth, and twentieth fringes were missing (Fig. 1).

There is a problem, however, in choosing an appropriate unit size for the array spacing. The results are affected by the number of array points that fall within the slits and their positions relative to the slits. By changing the array spacing a minute amount, one can pull one more array point in or out of the slit width, which can change the problem dramatically. In many cases every sixth fringe was missing instead of every fifth, and in one case every seventh fringe was missing. This is best understood by analyzing the problem the code is working, which is an approximation of the desired problem.

Using the above problem with slit widths b and separation a, the code will approximate these distances by putting a certain number of array points within the slits. The number is determined by the unit size. Let the two slits be centered about the origin, and the unit size or the distance between array points be u. Let the first and last points to fall within the slit be m and m + n respectively. Thus the slit width the code is actually using is the unit size times n. That is, it is not b but b' = nu, where the prime indicates the approximate values the code is using. The slit separation, which is measured from the midule of one slit to the middle of the other slit, is then a' = 2mu + nu. Hence the missing fringe will be given by:

$$M' = \frac{a'}{b'} = \frac{2m + n}{n}$$

In two separate cases the unit sizes were chosen to be .0020 cm and .0019 cm respectively for an array size of 256 x 256. For the first case, the code selected m = 10 as the first array point to fall within the slit, and the slit width encompassed five array points, ie. n = 5. Hence M' = 5, which is exactly the original problem. However, for the second case where n = .0019 cm, the code selected the first point to fall within the slit as m = 12 and the slit width was n = 4. Hence M' = 7, which means the seventh fringe was suddenly missing with only a slight change in the unit size.

For all the cases with a unit size smaller than u = .0015 cm, the missing fringe was always the fith one. This says that the smaller the unit size (or the greater the resolution) the more reliably the code can perform the problem, which stands to reason. For this particular problem, this translates into a requirement of at least seven points within the slit width.

The four-slit and six-slit problems were set up with the same slit width and slit separation as in the two-slit problem. Extra slits were added outside the original two. The expected results are very similar to the two-slit case except that the bright fringes become narrower. The fringe positions and the missing fringes should remain the same. Figure 2 shows the two-slit problem again except with a different unit size. This is included for comparison to the four- and six-slit problems with the same unit size, which are shown in Figs. 3 and 4. The GLAD results agree very well with the narrowing of the bright fringes and their positions. The missing fringes, however, were not totally absent, al-

though fringe number five does have a deep notch in it (see Fig. 3). This problem was more pronounced in the six slit case (see Fig. 4). Overall, though, agreement with theory is very good.

It can be concluded, from this first study, that the code does handle simple diffraction problems correctly. Since these classic problems have been verified by many experiments over the years it has been demonstrated that the code agrees well with experiment both in intensity and spatial distribution. There are problems, however. Due to practical limits on the array size, the code lacks the resolution required to model high spatial frequency gratings.

Modeling Ripple on Liquid-Cooled Mirrors

The mirrors of high powered FELs will experience power densities high enough to damage ordinary mirror surfaces. Therefore an effort is underway to design, analyze, and build mirrors that are cooled by flowing a fluid through a substructure under the mirror surface. The results to date of the analysis performed on the code GLAD are presented in this section.

The mirror design considered for this analysis assumes that the substructure consists of a grid of square cells through which the fluid will flow. A high powered beam will cause a certain amount of distortion of the mirror surface. The square grid substructure will, consequently, show through on the surface as linear ripple in two directions across the mirror surface. This may be thought of as a very low frequency, sinusoidal grating.

The resonator used in this analysis is described in detail in reference 1. Briefly, though, it consists of two spherical, normal incidence mirrors and one grazing incidence, off-axis, hyperboloidal, beam expanding mirror (see Fig. 5). The grazing incidence angle is about 86°. The right hand sphere is positioned so that its radius of curvature is coincident with the focus B of the hyperbola, so that the beam is intercepted at normal incidence and returned back on itself. Therefore, the radius of curvature of the sphere is imaged at focus A of the hyperbola. The radius of curvature of the left hand sphere overlaps the image at focus A thus creating a near concentric resonator. The waist appears within the overlap region at position ω_o. The overall length of the resonator is approximately 64 m. The wavelength used in this analysis is 0.6328 μm. For a stable Gaussian mode, ω_o = 0.0663 cm was used (ω_o is the beam half width at $1/e^2$ of the intensity).

For this study, ripples are added to the right hand sphere and to the grazer; but none to the left hand sphere. The grid structure of the sphere is made up of 1/4 inch squares and that of the grazer is 1/8 inch squares. Hence, the periods of the sinusoidal ripple are 1/4 inch and 1/8 inch respectively for the two mirrors.

Adding the ripple to the sphere is very straightforward since the beam is normally incident on the mirror. However, for the grazer it is complicated by the extreme grazing incidence angle. The ripple in one transverse direction will be foreshortened and hence will appear to the beam to have a much higher spatial frequency than in the other transverse direction. The amplitude of the wavefront error, however, will be reduced uniformly across the surface of the mirror by the tilt of the grazing incidence angle (a factor of cos 86°). Thus the tolerance on figure error for the grazer does not have to be as tight as for the sphere. The period of the foreshortened ripple is about 0.021 cm, which is approximately half of the spacing for the slits in the previous section of classical problems; therefore an array of double the size (512 x 512) was used for the ripple study.

One last subject that must be discussed before the results can be presented is the resolution in both the near and far field. The unit size is chosen initially at the beam waist where the wavefront is flat. The unit size in the far field (at either mirror position) is then determined by the code using the formula: $u' = \lambda z/Nu$ (a result of Fourier Transform Theory). The unit sizes in the near and far fields are u and u', λ is the wavelength, z is the distance propagated, and N is the array size. This is an inverse relation which says that for greater resolution in the far field one gives up resolution in the near field and vice versa. The code has an automatic mode for the choice of the initial unit size such that the resolution in both the near and far fields are equal. For the present study, this mode was not employed, because greater resolution was required at the mirrors. Care must be taken when doing this, because aliasing can become a problem.

A case of an unaberrated resonator was run for one hundred passes to demonstrate that a stable Gaussian mode exists; this run agreed well with analytical calculations. The results of the ripple study are from cases based on the waist parameters of this stable mode. These cases are, however, run for only a single round trip pass. This study, therefore, indicates how a stable mode is affected by the ripple added to these two mirrors for a single pass. Since the resolution was not the same in the near and far fields, it was felt that the results of multipass runs would be questionable, so none were run. For the unaberrated case the resolution was allowed to be equal in both the near and far fields.

Two cases will be discussed here. The first assumed the same surface error due to ripple on both mirrors (1/20 wave peak to valley) and for the second case a more restrictive tolerance was placed on the sphere (1/100 wave peak to valley), while the grazer remained the same.

Figure 6 shows the results at the waist for the first case. It shows the diffraction pattern due to ripple on both the grazer and the sphere. The x and y axes are transverse to the beam propagation direction. To satisfy the Nyquist sampling criteria (of at least 4 array points under each period of the sinusoidal ripple), greater resolution was required at both mirrors. This implies lower resolution in the near field (at the waist). That is why, in Fig. 6, the Gaussian-like beam appears as a spike in the center of the three-dimensional plot. A 512 x 512 array was used for this problem and the array spacing was u = .06 cm at the waist ω_o. Figures 6-12 are all based on this array size and spacing and all

have been cropped off at 8 cm. The field size for this array is about 15 cm (where the origin is in the center of the array).

Meeting the Nyquist criteria for the ripple on the sphere was easily accomplished, but for the foreshortened axis of the grazer to meet the criteria, a 512 x 512 array was required. By analyzing the results in Figs. 6-9, one finds that all the diffraction lobes are identifiable. The four spikes in Fig. 6 that are equidistant from the central beam are due to the ripple on the sphere. They are at a distance r_1 = 1.54 cm from the center. The two smaller spikes, in close to the central beam and along the x axis, result from the untilted transverse axis of the grazer. These spikes can also be seen in Fig. 7 which is a "slice" through the three-dimensional plot along the x axis (y=0). The solid line is a plot of the intensity at the waist and the dashed line is a plot of the phase. The vertical scale has been chosen to emphasize the low intensity diffraction lobes; hence the main beam is off scale. The peak intensity is indicated in the margin. In Fig. 8 the diffraction lobes due to the tilted transverse axis of the grazer are found near the edge of the plot at about r = 7.5 cm. Figure 8 is a "slice" along the y axis of Fig. 6.

Figure 9 is a power-in-the-bucket plot and sums up the power in circular rings of increasing radii that are centered on the main beam. The total power has been normalized to one so that the fractional power is displayed on the vertical axis, and the horizontal axis is the distance from the center of the beam. Each set of spikes that is equidistant from the center of the beam appears as a step in this plot. The main beam has 66% of the power in it, which accounts for the initial step up to .659. The first step to the right of that, to .663, is caused by the two spikes on the x axis, which are caused by the ripple of the untilted axis of the grazer. The step due to the tilted axis is found on the extreme right hand side of Fig. 9, as a small step at approximately r = 7.5 cm.

The remainder of the steps result from the ripple on the sphere. The four largest diffraction lobes account for the largest step (from .663 to .953). Each of the next two steps to the right of that are caused by a set of very faint lobes at equal radii, which when taken together add up to the small step. They lie on a grid of squares with sides of dimension r_1 = 1.54 cm, so that they fall on diagonals out from the central beam at distances of $r_1\sqrt{2}$ and $r_1\sqrt{5}$. Because of their very low individual power, they do not show up well on the intensity plots.

All of the power thrown out into the diffraction pattern represents a loss in the laser resonator. For the case shown in Figs. 6-9, this is approximately a 34% loss per pass. For the case shown in the next plots, Figs. 10-12, the tolerance on the sphere was decreased to 1/100 wave of surface error (peak to valley). Figures 10 and 11 show the x and y axis of the beam at the waist and the substantially reduced diffraction pattern. Figure 12 shows the power-in-the-bucket plot for this case and a significant improvement in the loss, which is about 3% loss per pass. To separate the effects of the two mirrors, the ripple was placed only on the grazer for the case shown in Fig. 13 and only on the sphere for the case shown in Fig. 14. The two steps seen in Fig. 13 are due to the two different spatial frequencies of ripple on the grazer and the single step in Fig. 14 is due to the one frequency of ripple placed on the sphere.

The conclusion drawn from this study is that GLAD can model ripple of the cooled mirrors very well. Furthermore, ripple can cause a significant loss in the laser resonator, and the sphere is the more sensitive of the two mirrors in this problem. It should be pointed out that the 3% loss per pass is a worst case, because the ripple was applied uniformly across the mirrors in the calculations. In reality, since the ripple is a function of the beam intensity and since the beam would be approximately Gaussian, the amplitude of the ripple will be greatest at the center of the beam and will fall off to near zero in the wings.

Conclusion

From the studies presented in this paper, it can be concluded that the code GLAD handles diffraction problems correctly. Its results compare very well with classical text book solutions. The code was used to analyze the problem of ripple on liquid-cooled mirrors with a square grid substructure. The results show that for a practical, efficient FEL resonator, ripple will have to be controlled very well. Ripple will also be a more serious proolem for the normal incidence mirrors than for the grazing incidence mirrors.

References

1. C. E. Knapp, V. K. Viswanathan, S. C. Bender, Q. D. Appert, G. Lawrence, and C. Barnard. "Analysis of FEL optical systems with grazing incidence mirrors," Proceedings of S. P. I. E., Vol. 642, pp. 214-221, 1986.

2. G. Lawrence, C. Barnard, and V. K. Viswanathan. "Global Coordinates and Exact aberration calculations applied to physical optics modeling of complex optical systems, "Proceedings of S. P. I. E., Vol. 642, pp. 173-179, 1986.

3. M. Born, E. Wolf, Principles of Optics, 6th ed., Pergamon Press, pp. 393-407, 1984.

4. E. Holt, Schaum's Outline Series Theory and Problems of Optics, McGraw-Hill, Inc., pp. 159-179, 1975.

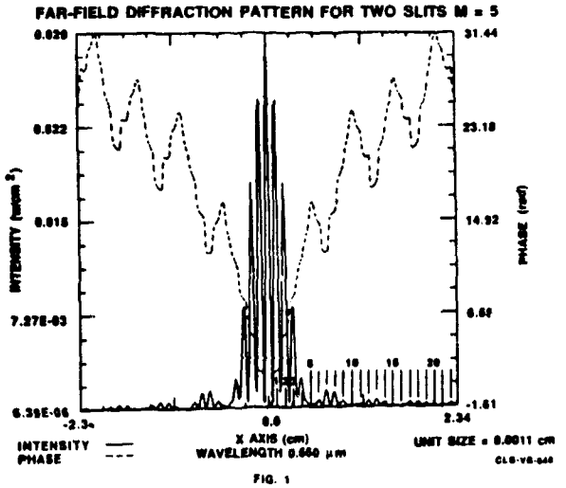

FIG. 1

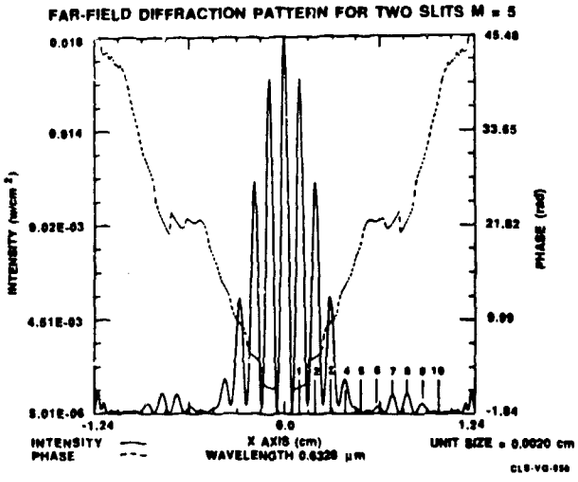

FIG. 2

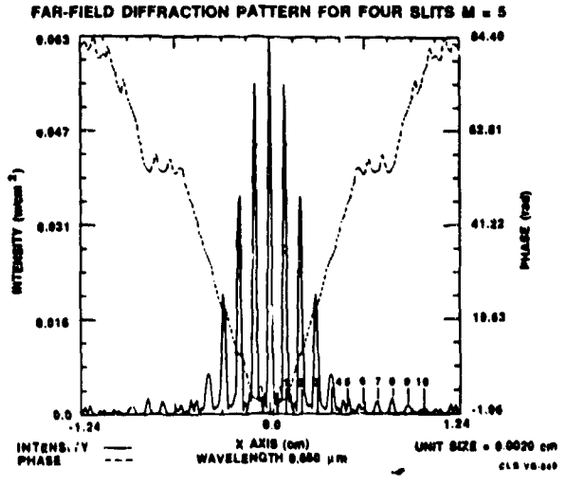

FIG. 3

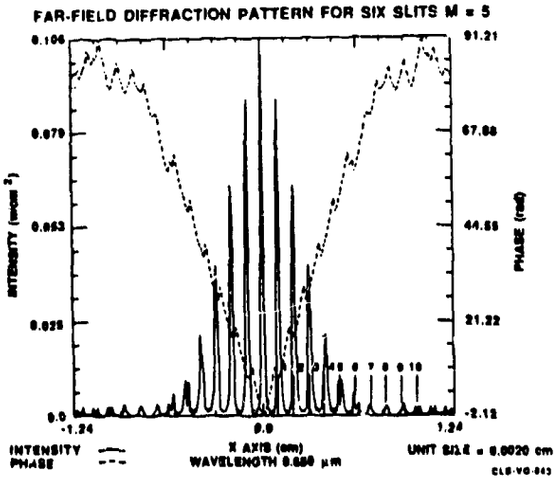

FIG. 4

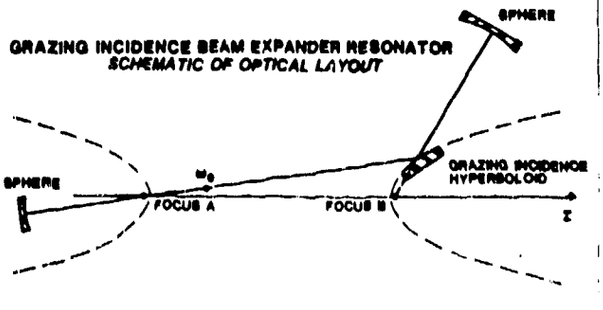

FIG. 5

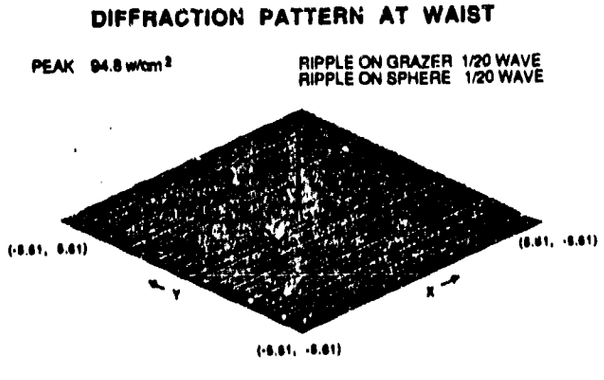

FIG. 6

SLS-VG-1008

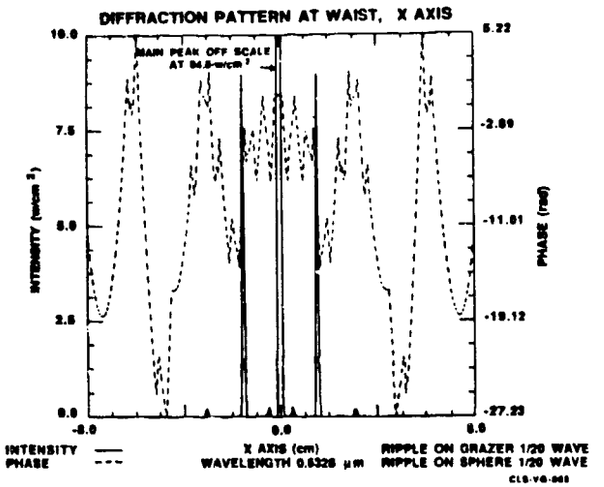

FIG. 7

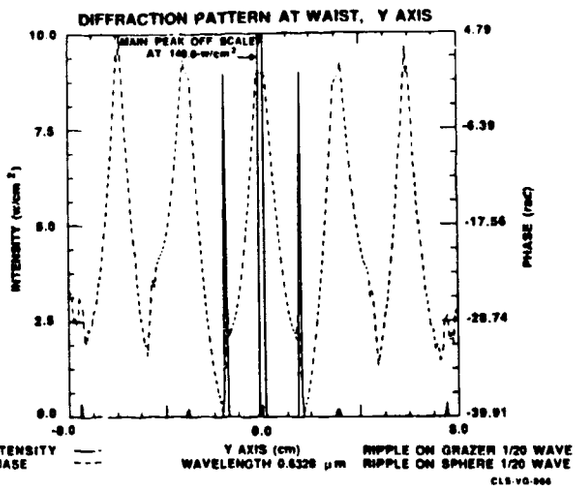

FIG. 8

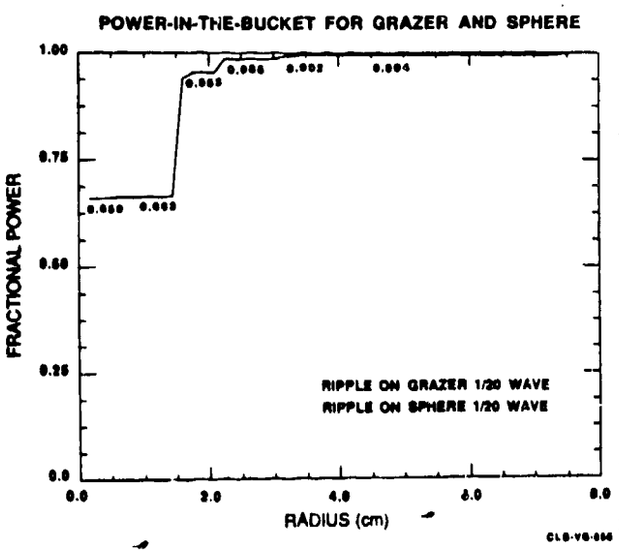

FIG. 9

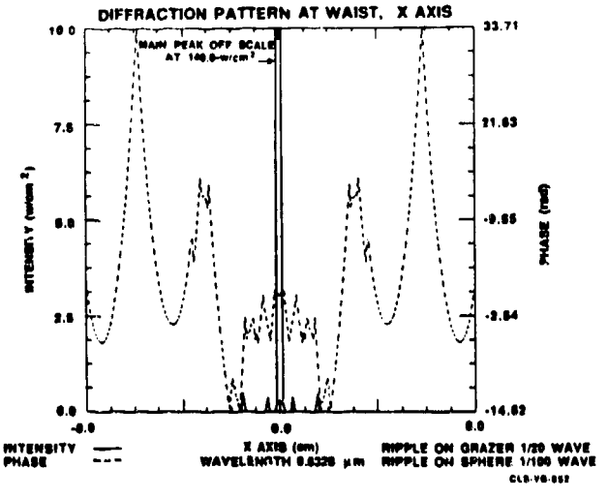

FIG. 10

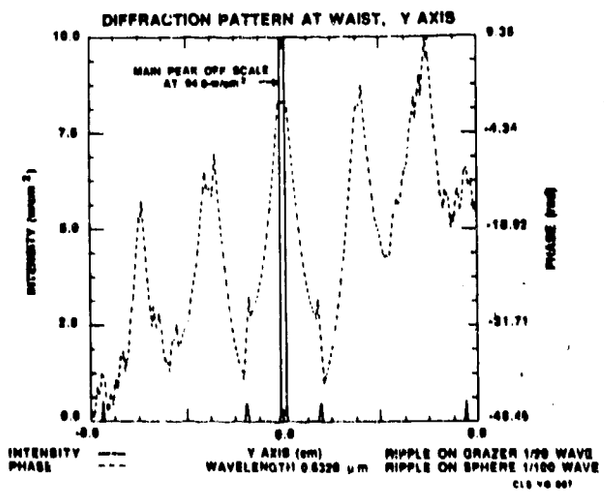

FIG. 11

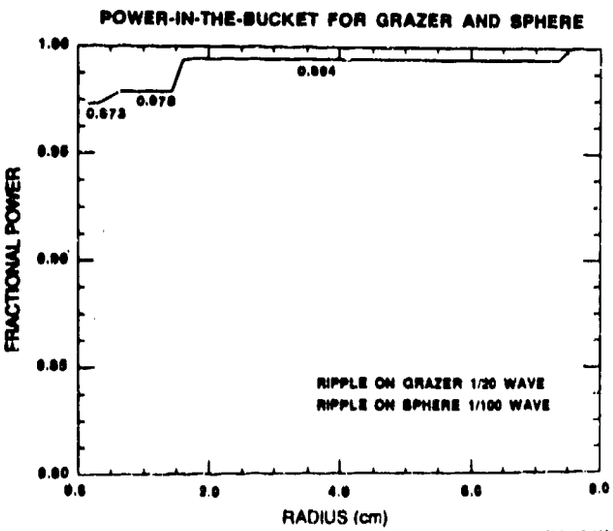

FIG. 12

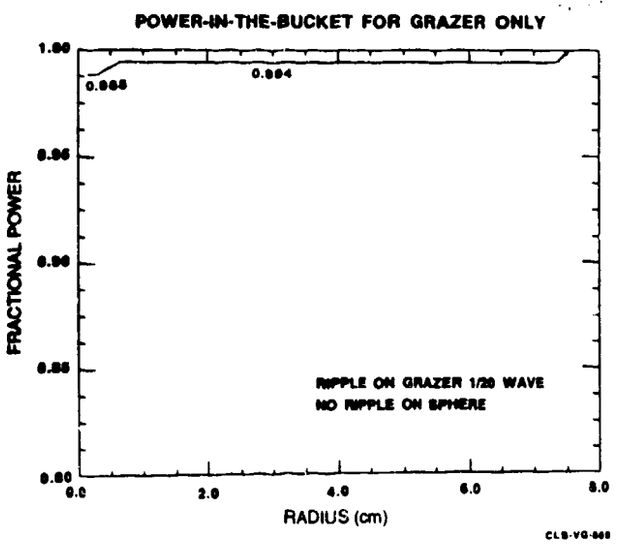
POWER-IN-THE-BUCKET FOR GRAZER ONLY
FRACTIONAL POWER
1.00
0.95
0.90
0.85
0.80
0.994
0.994
RIPPLE ON GRAZER 1/20 WAVE
NO RIPPLE ON SPHERE
0.0
2.0
4.0
6.0
8.0
RADIUS (cm)

FIG. 13

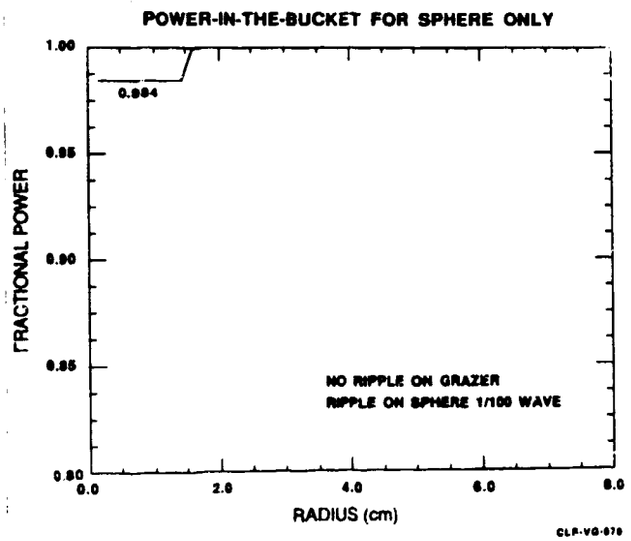
POWER-IN-THE-BUCKET FOR SPHERE ONLY
FRACTIONAL POWER
1.00
0.95
0.90
0.85
0.80
0.994
NO RIPPLE ON GRAZER
RIPPLE ON SPHERE 1/100 WAVE
0.0
2.0
4.0
6.0
8.0
RADIUS (cm)

FIG. 14